THE JOURNAL OF BIOLOGICAL CHEMISTRY VOL. 281, NO. 13, pp. 8628–8635, March 31, 2006

Function and Solution Structure of Huwentoxin-X, a Specific Blocker of N-type Calcium Channels, from the Chinese Bird Spider *Ornithoctonus huwena*[*]

Received for publication, December 20, 2005, and in revised form, January 26, 2006 Published, JBC Papers in Press, January 26, 2006, DOI 10.1074/jbc.M513542200

Zhonghua Liu[‡], Jie Dai[§], Longjun Dai[§], Meichun Deng[§], Zhe Hu[§], Weijun Hu[§], and Songping Liang[‡§1]

From the [‡]College of Life Sciences, Peking University, Beijing 100087 and the [§]College of Life Sciences, Hunan Normal University, Hunan 410081, China

Huwentoxin-X (HWTX-X) is a novel peptide toxin, purified from the venom of the spider *Ornithoctonus huwena*. It comprises 28 amino acid residues including six cysteine residues as disulfide bridges linked in the pattern of I–IV, II—V, and III–VI. Its cDNA, determined by rapid amplification of 3′ and 5′ cDNA ends, encodes a 65-residue prepropeptide. HWTX-X shares low sequence homology with ω-conotoxins GVIA and MVIIA, two well known blockers of N-type Ca^{2+} channels. Nevertheless, whole cell studies indicate that it can block N-type Ca^{2+} channels in rat dorsal root ganglion cells (IC_{50} 40 nM) and the blockage by HWTX-X is completely reversible. The rank order of specificity for N-type Ca^{2+} channels is GVIA ≈ HWTX-X > MVIIA. In contrast to GVIA and MVIIA, HWTX-X had no detectable effect on the twitch response of rat vas deferens to low frequency electrical stimulation, indicating that HWTX-X has different selectivity for isoforms of N-type Ca^{2+} channels, compared with GVIA or MVIIA. A comparison of the structures of HWTX-X and GVIA reveals that they not only adopt a common structural motif (inhibitor cystine knot), but also have a similar functional motif, a binding surface formed by the critical residue Tyr, and several basic residues. However, the dissimilarities of their binding surfaces provide some insights into their different selectivities for isoforms of N-type Ca^{2+} channels.

Ca^{2+} entry into cells through voltage-gated Ca^{2+} channels mediates many physiological processes including neurotransmitter release, neurosecretion, neuronal excitation, survival of neurons, and regulation of gene expression. Currently, five main types of Ca^{2+} channels (T, L, N, P/Q, and R) in vertebrate cells have been defined by their physiological and pharmacological properties (1–3). Among the multiple types of Ca^{2+} channels, N-type Ca^{2+} channels are sensitive to ω-conotoxin GVIA that is derived from the sea snail *Conus geographus*, and are concentrated at presynaptic nerve termini, regulating the influx of Ca^{2+} necessary for neurotransmitter release in both the central and peripheral nervous systems (4–6). Several different isoforms of N-type Ca^{2+} channels have now been cloned and functionally characterized (7, 8). Pharmacological and gene knock-out studies implicate N-type Ca^{2+} channels as key mediators of nociceptive signaling in dorsal root ganglion (DRG)[2] cells, and therefore as potential targets for the development of analgesic drugs (9). Indeed, ziconotide, a synthetic analog of ω-conotoxin MVIIA that is also a specific N-type Ca^{2+} channels blocker isolated from the venom of the marine snail *Conus magus*, has received approval for severe chronic pain resistant to other procedures (10, 11). Another more selective blocker of N-type Ca^{2+} channels, ω-conotoxin CVID isolated from *C. magus*, is currently in Phase II clinical trials in Australia. It is hoped that this peptide may overcome some of the side effects associated with MVIIA use (12–15).

The most specific blockers of N-type Ca^{2+} channels known to date are isolated from the venoms of cone snails. Only a few peptide toxins from other animals have been reported to be able to act specifically on this type of channels, such as Ptu1, isolated from the venom of assassin bugs *Peirates turpis* (16), and HWTX-I, isolated from the venom of spider *Ornithoctonus huwena* (17). It is well known that spiders are among the oldest animals on the earth. There are 38,000 described spider species, with at least a similar number uncharacterized. A very conservative estimate of 20 pharmacologically distinct peptides per species leads to an estimated total of ~1.5 million spider venom peptides, which is much larger than the ~50,000 peptides estimated to be present in venoms of cone snails (18). Thus it is reasonable to believe that the spider venoms might contain a number of peptide probes that are more specific for isoforms of N-type Ca^{2+} channels. These peptides might aid to discriminate among their isoforms and would become ideal drug candidates for treatment of N-type Ca^{2+} channel-related disorders.

The Chinese bird spider, *O. huwena*, is found mainly in the hilly areas of Yunnan and Guangxi provinces in the south of China (19). More than 10 peptide toxins have been isolated from this spider venom, including the N-type Ca^{2+} channel inhibitor (HWTX-I) (17), insecticidal neurotoxins (HWTX-II, HWTX-VII, and HWTX-VIII) (20, 21), tetrodotoxin-sensitive Na^{+} channel blocker (HWTX-IV) (22), the smallest lectin-like peptide (SHL-I) (23), and others. In the present study, we report the isolation and characterization of huwentoxin-X (HWTX-X) from the venom of *O. huwena*, a novel specific blocker of N-type Ca^{2+} channels in rat DRG cells. cDNA sequencing by rapid amplification of the 3′ and 5′ cDNA ends (RACE) method indicates HWTX-X is initially expressed as a prepropeptide, an expression pattern similar to other spider peptide toxins and conotoxins. The determination of the solution structure of HWTX-X by two-dimensional ^{1}H NMR with distance geometry and simulated annealing reveals that HWTX-X adopts the same inhibitor cystine knot motif seen in ω-conotoxins (*e.g.* GVIA or MVIIA).

* This work was supported by National Natural Science Foundation of China Contract 30430170. The costs of publication of this article were defrayed in part by the payment of page charges. This article must therefore be hereby marked "*advertisement*" in accordance with 18 U.S.C. Section 1734 solely to indicate this fact.

The atomic coordinates and structure factors (code 1Y29) have been deposited in the Protein Data Bank, Research Collaboratory for Structural Bioinformatics, Rutgers University, New Brunswick, NJ (http://www.rcsb.org/).

[1] To whom correspondence should be addressed. Tel.: 86-731-8872556; Fax: 86-731-8861304; E-mail: liangsp@hunnu.edu.cn.

[2] The abbreviations used are: DRG, dorsal root ganglion; HWTX-X, huwentoxin-X; RACE, rapid amplification of cDNA ends; RP-HPLC, reverse-phase high performance liquid chromatography; MALDI-TOF, matrix-assisted laser desorption ionization time-of-flight; MS, mass spectrometry; HVA, high voltage-activated; HOBt/TBTU/NMM, hydroxybenzotriazole monohydrate/2-(1*H*-benzotriazol-1-yl)-1,2,3,3-tetramethyluronium tetrafluoroborate/*N*-methylmorpholine.

EXPERIMENTAL PROCEDURES

Materials and Animals—Kunming albino mice and Sprague-Dawley rats were purchased from the Xiangya School of Medicine, Central South University. Cockroaches were from our laboratory stock colonies. All sequencing reagents were purchased from Applied Biosystems (Foster City, CA). The 3′ and 5′ RACE kits and TRIzol reagent were purchased from Invitrogen. Restriction enzymes, *Taq* DNA polymerase, and pGEMT Easy Vector system were from Promega. All synthesis reagents were purchased from Chemassist Corp. Trifluoroacetic acid and α-cyano-4-hydroxycinnamic acid were from Sigma. All other reagents are analytical grade.

Toxin Purification—The venom was obtained by electrical stimulation of female spiders, and the freeze-dried crude venom was stored at −20 °C prior to analysis. Lyophilized venom, dissolved in double-distilled water, was applied onto a reverse-phase high performance liquid chromatography (RP-HPLC) Vydac C18 column (300 Å, 4.6 × 250 mm) using a Waters Alliance system. Venom components were eluted using a linear acetonitrile gradient (0–60% acetonitrile, 0.1% trifluoroacetic acid in 60 min) at a flow rate of 1.0 ml/min. Elution of peptides was monitored at 215 nm.

Mass Spectrometry—The molecular masses of peptides were determined using MALDI-TOF MS (Applied Biosystems, Voyager-DE STR Biospectometry work station). Ionization was achieved by irradiation with a nitrogen laser (337 nm), with a 20-kV acceleration voltage. α-Cyano-4-hydroxycinnamic acid was used as matrix. Prior to each analysis in the reflection mode, the masses were calibrated internally using HWTX-I (MH^+, 3751.45 Da).

Amino Acid Sequencing by Automated Edman Degradation—The native or carboxymethylated peptide was submitted to automatic N-terminal sequencing on an Applied Biosystems model 491 gas-phase sequencer. Edman degradation was performed with a normal automatic cycle program.

HWTX-X cDNA Isolation and Characterization—The full-length HWTX-X cDNA was obtained using the RACE method as described previously (24). Briefly, 5 μg of mRNA, extracted from the venomous glands of the spider *O. huwena*, was taken to convert mRNA into cDNA by using the 3′ RACE kit supplied with Superscript II reverse transcriptase and a universal adapter primer (5′-GGCCACGCGTCGACTAGTAC(dT)-3′). The cDNA was then used as a template for PCR amplification using the abridged universal adapter primer (5′-CGAAGCTTGGCCACGCGTCGACTAGTAC-3′) and the gene specific primer (5′-GG(A/G/C/T)AA(A/G)CC(A/G/C/T)TG(C/T)TA(C/T)GG(A/G/C/T)-3′) designed corresponding to the N-terminal residues (Gly^6-Lys-Pro-Cys-Tyr-Gly^{11}) of HWTX-X. Based on the partial cDNA sequence of HWTX-X determined by 3′ RACE, an antisense primer was designed and synthesized for 5′ RACE. With the strategy described by the RACE kit supplier, the 5′-end cDNA of HWTX-X was cloned by using the gene-specific primer (5′-GTGAACACACTCCGCAGCAC-3′) and nested primer, respectively. The amplified products were then precipitated and cloned into the pGEM-T easy vector for sequencing.

Peptide Synthesis, Folding, and Purification—HWTX-X was synthesized using an Fmoc (*N*-(9-fluorenyl)methoxycarbonyl)/*tert*-butyl strategy and HOBt/TBTU/NMM coupling method on an automatic peptide synthesizer (PerSeptive Biosystems) (25). The crude linear peptide was diluted to a final concentration of 30 μM by 0.1 M Tris-HCl solution (pH 8.0) containing 5 mM reduced glutathione and 0.5 mM oxidized glutathione. The solution was stirred slowly at room temperature for 24 h and the folding reaction was monitored by RP-HPLC and MALDI-TOF MS. The oxidized product was purified by semipreparative RP-HPLC using a 40-min linear acetonitrile gradient (10–30% acetonitrile, 0.1% trifluoroacetic acid) on a column (C18, 1.0 × 25 cm) at 3 ml/min flow rate. The purity of the synthetic HWTX-X was confirmed by analytical RP-HPLC and MALDI-TOF MS.

Biological Assays—The toxicity of HWTX-X was qualitatively assayed by intraperitoneal injection into 18–20-g mice of both sexes and intra-abdominal injection into adult male cockroaches (*Periplaneta americana*) with body weights of 0.3–0.5 g using 20-μl solutions (in 0.9% (w/v) normal saline). Vas deferens assays were performed according to the method of Liang (26). Briefly, adult male Sprague-Dawley rats were killed by CO_2 anesthesia followed by decapitation. Vas deferentia were mounted in 5-ml organ baths, with the top of each tissue attached to an isometric force transducer and the bottom attached to a movable support and straddled with platinum stimulating electrodes. The vasa were immersed in Krebs solution and stretched by a passive force of about 10 millinewtons. After an equilibration period of 30 min with frequent changes of medium, the vasa were stimulated with single electrical field pulses (30 V, 0.1 ms duration) every 20 s. The resulting twitch responses mediated by sympathetic nerves were recorded on a chart recorder (RM6240B).

Electrophysiological Assays—Acutely dissociated DRG cells were prepared from 4-week-old Sprague-Dawley rats and maintained in short-term primary culture using the method described by Hu *et al.* (27). The dissociated cells were suspended in essential Dulbecco's modified Eagle's medium supplemented with 10% fetal bovine serum, 50 IU/ml penicillin, and 50 μg/ml streptomycin. The cells were plated on a poly-L-lysine-coated dish (35 × 10 mm) and incubated at 37 °C in an atmosphere of 5% CO_2. Cells in culture for 3–24 h were used in the patch experiments. Experiments were conducted at room temperature (20–25 °C).

Cell current recordings were made with the whole cell patch clamp technique using an EPC-9 patch clamp amplifier (HEKA Electronid, Lambrecht, German). Voltage steps and data acquisition were controlled using a PC computer with software Pulsefit+Pulse 8.0 (HEKA Electronics, Lambrecht, Germany). The patch pipettes with DC resistances of 2–3 MΩ were fabricated from borosilicate glass tubing (VWR micropipettes, 100 μl, VWR Company) using a two-stage vertical microelectrode puller (PC-10, Narishige, Japan) and fire-polished by a heater (Narishige, Japan). Data were sampled at 10 KHz and filtered at 3 KHz. Under the voltage clamp 70–80% series resistance compensation was applied.

Ca^{2+} channel currents ($I_{Ca^{2+}}$) were measured using Ba^{2+} as a charge carrier ($I_{Ba^{2+}}$). For these experiments, external solutions contained (in mM): 160 triethanolamine-Cl, 10 HEPES, 2 $BaCl_2$, 10 glucoses, and 200 nM tetrodotoxin, adjusted to pH 7.4 with triethanolamine-OH. The internal solution contained (in mM): 120 $CsCl_2$, 5 Mg-ATP, 0.4 Na_2-GTP, 10 EGTA, 20 HEPES-CsOH (pH 7.2) (13–15). $I_{Ba^{2+}}$ was evoked at −50 or 0 mV from a holding potential of −90 or −40 mV. HWTX-X, ω-conotoxin GVIA, MVIIA, nifedipine, and $NiCl_2$ were applied to the extracellular environment by low pressure ejection from a blunt pipette positioned about 50–100 μm away from the cell being recorded. Data were given as mean ± S.E. and statistical significance ($p < 0.05$) was determined using a paired or independent Student's *t* test as appropriate.

NMR Spectroscopy of HWTX-X—The NMR sample was prepared by dissolving HWTX-X in 450 μl of 20 mM deuterium sodium acetate buffer (H_2O/D_2O, 9:1, v/v) containing 0.002% NaN_3 and 0.01 mM EDTA with a final concentration of 6 mM HWTX-X and a pH of 4.0. Sodium 3-(trimethylsilyl) propionate-2,2,3,3-d_4 was added to a final concentration of 200 μM as an internal chemical shift reference. For experiments in D_2O, the sample used in H_2O experiments was lyophilized and then

redissolved in 450 μl of 99.996% D_2O (Cambridge Isotope Laboratories). All NMR spectra were observed on a 500-MHz Bruker DRX-500 spectrometer with a sample temperature of 298 K. Several sets of two-dimensional spectra were recorded in a phase-sensitive mode by the time-proportional phase increment method following standard pulse sequences and phase cycling. TOCSY spectra were obtained with a mixing time of 85 ms. NOESY spectra were recorded in D_2O with a mixing time of 200 ms and in H_2O with mixing times of 100, 200, and 400 ms. Solvent suppression was achieved by the presaturation method. All two-dimensional measurements were recorded with 1024–512 frequency data points and were zero-filled to yield 2048–1024 data matrices except for the high resolution DQF-COSY spectrum. The DQF-COSY spectrum was recorded with 2048–1024 data points in the t2 and t1 dimensions, respectively, and zero-filled to 4096–2048 points to measure the coupling constants. All spectra were processed and analyzed using Felix 98.0 (Biosym Technologies) software running on a Silicon Graphics O_2 work station. Before Fourier transformation, the signal was multiplied by a sine bell or sine bell square window functions with a $\pi/2$ phase shift.

Structure Calculations—Distance constraints were obtained from the intensities of cross-peaks in NOESY spectra with a mixing time of 200 ms. All NOE data were classified into four distance ranges, 1.8–2.5, 1.8–3.0, 1.8–4.0, and 1.8–5.0 Å, corresponding to strong, medium, weak, and very weak NOE values, respectively. According to the method (28), if the connectivity involved side chain protons, 3.0-, 4.0-, and 5.0-Å upper bounds were used instead to account for higher mobility. For sequential $d\alpha$N and dNN connectivities, we used bounds of 2.5-, 3.0-, and 4.0-Å, respectively. Pseudo-atom corrections were applied to non-stereospecifically assigned methyl and methylene protons according to the method of Wüthrich (38). Ten dihedral angle restraints derived from $^3J_{\mathrm{NH\text{-}C\alpha H}}$ coupling constants were restrained to $-120 \pm 30°$ for $^3J_{\mathrm{NH\text{-}C\alpha H}} \geq 8.80$ Hz and $-65 \pm 25°$ for $^3J_{\mathrm{NH\text{-}C\alpha H}} \leq 5.5$Hz. Three distance constraints were added to each disulfide bridge that was mainly determined from NMR data. The corresponding distances were 2.02 ± 0.02, 2.99 ± 0.5, and 2.99 ± 0.5 Å for $S(i) - S(j)$, $S(i) - C_\beta(j)$, and $S(j) - C_\beta(i)$, respectively. Structure calculations of HWTX-X were run on a Silicon Graphics work station using the standard protocol of the X-PLOR-NIH 2.9.6 program (29).

RESULTS

Purification Characterization and Synthesis of HWTX-X—Crude venom from the spider *O. huwena* was fractionated by RP-HPLC on a Vydac C18 column (Fig. 1*A*). More than 20 peaks were observed in the chromatogram. The sharp peak labeled HWTX-X, eluted at 13 min at a point in the gradient of about 18% acetonitrile, 0.1% trifluoroacetic acid, was found to block N-type Ca^{2+} channels in rat DRG cells. As assessed by mass spectrometry, the purified fraction contained one component, whose average molecular mass $(M + H)^+$ was determined as 2,931.34 Da. The purity of HWTX-X was over 98%, as judged by RP-HPLC and N-terminal sequence analysis. The complete amino acid sequence of HWTX-X was derived by Edman degradation (fig. 2), revealing it as a 28-amino acid polypeptide containing six cysteine residues. The molecular mass of HWTX-X determined by mass spectrometry was 6 Da less than that calculated from its amino acid sequence, assuming all 6 cysteine residues are involved in disulfide bridges. Primary structure analysis of HWTX-X highlights that a basic peptide with four basic residues (Lys^1, Lys^7, Lys^{15}, and Lys^{24}) but no acidic residues, HWTX-X, is also a rather polar peptide containing only seven hydrophobic residues, which is consistent with its relatively short retention time in the RP-HPLC.

The amino acid sequence of HWTX-X was used to search the protein data base for possible homologues using an online BLAST search. HWTX-X has low sequence homology with other huwentoxins, but it shares ~50% homology with two Ca^{2+} channel blockers, namely Ptu1 (34 residues) isolated from the venom of assassin bugs *P. turpis* (16, 30) and ω-conotoxin SVIA (24 residues) isolated from the venom of *Conus striatus* (Fig. 2) (31). When the amino acid sequences of HWTX-X and ω-conotoxins GVIA, MVIIA, and CVID were aligned, it was found that sequence homology between HWTX-X and these ω-conotoxins is low (<32%), but they indeed share some similarities. The four peptides are basic and they all have six conserved Cys residues that are arranged to give a four-loop Cys framework (C-C-CC-C-C). Moreover, among other amino acid residues, they contain the well conserved neutral residue Gly^6 and the basic residues Lys^{26} or Arg^{26} (HWTX-X numbering) (Fig. 2), which are also conserved throughout all ω-conotoxins. These similarities represent substantial clues for investigating the bioactivity of HWTX-X in Ca^{2+} channels.

Because of the low amount of HWTX-X in the crude venom of *O. huwena*, this peptide was synthesized and then renatured, which yielded a major product as revealed by RP-HPLC and MALDI-TOF spectrometry (Fig. 1, *inset*). The purified product was homogeneous on the analysis by reverse-phase HPLC, and its mass (2931.45 Da) was in good accordance with the theoretical mass for the oxidized analog. Furthermore, the synthetic HWTX-X was able to block N-type Ca^{2+} channels in DRG cells similarly to the native peptide as determined by the patch clamp technique. Because the synthetic HWTX-X seemed to be structurally and functionally identical to the native toxin, it might be used for the further studies.

The cDNA Sequence of HWTX-X—The full-length cDNA sequence of HWTX-X was obtained by overlaying two fragments from the 3′ and 5′ RACE. As shown in Fig. 3, the oligonucleotide sequence of the cDNA is 486 bp comprising the 5′-untranslated region, the open reading frame, and the 3′-untranslated region. The open reading frame encodes a 65-residue peptide corresponding to the precursor of HWTX-X, which contains a signal peptide of 20 residues, a propeptide of 17 residues, and a mature peptide of 28 residues. The prepropeptide of the HWTX-X precursor shows limited sequence identity with those of other reported precursors. Different from most ω-conotoxins, HWTX-X has no extra amino acid Gly or Gly + Arg/Lys residues at its C terminus, known to allow "post-modification" of α-amidation at the C-terminal residue (49), implying that the C-terminal residue of mature toxin is not amidated.

Biological Assays—HWTX-X elicited no toxic symptoms in either vertebrates or invertebrates during a period of 48 h post-injection, when it was assayed *in vivo* by direct injection into mice and cockroaches. ω-Conotoxins (*e.g.* GVIA, MVIIA, and CVID) are known to block the twitch response to low frequency electrical nerve stimulation in rat vas deferens (3, 32). Because of the similarities between HWTX-X and these ω-conotoxins, similar pharmacological experiments were carried out to test the effect of HWTX-X on this tissue. In all the experiments conducted ($n = 10$), addition of 10 μM HWTX-X to the bath had no effect on the twitch response of vas deferens during 30 min, but 1 μM GVIA or MVIIA caused a rapid reduction of the twitch response, in agreement with previous studies (3, 32) (data not shown).

Effect of HWTX-X on Ca^{2+} Channels in Rat DRG Cells—It is widely accepted that rat DRG cells exhibit two categories of voltage-gated Ca^{2+} channels: low voltage-activated channels (T-type) and high voltage-activated (HVA) channels (N-, L-, P/Q-, and R-types), which can be discriminated by their voltage dependence and kinetics. Low voltage-activated currents can be elicited by a 100-ms step depolariza-

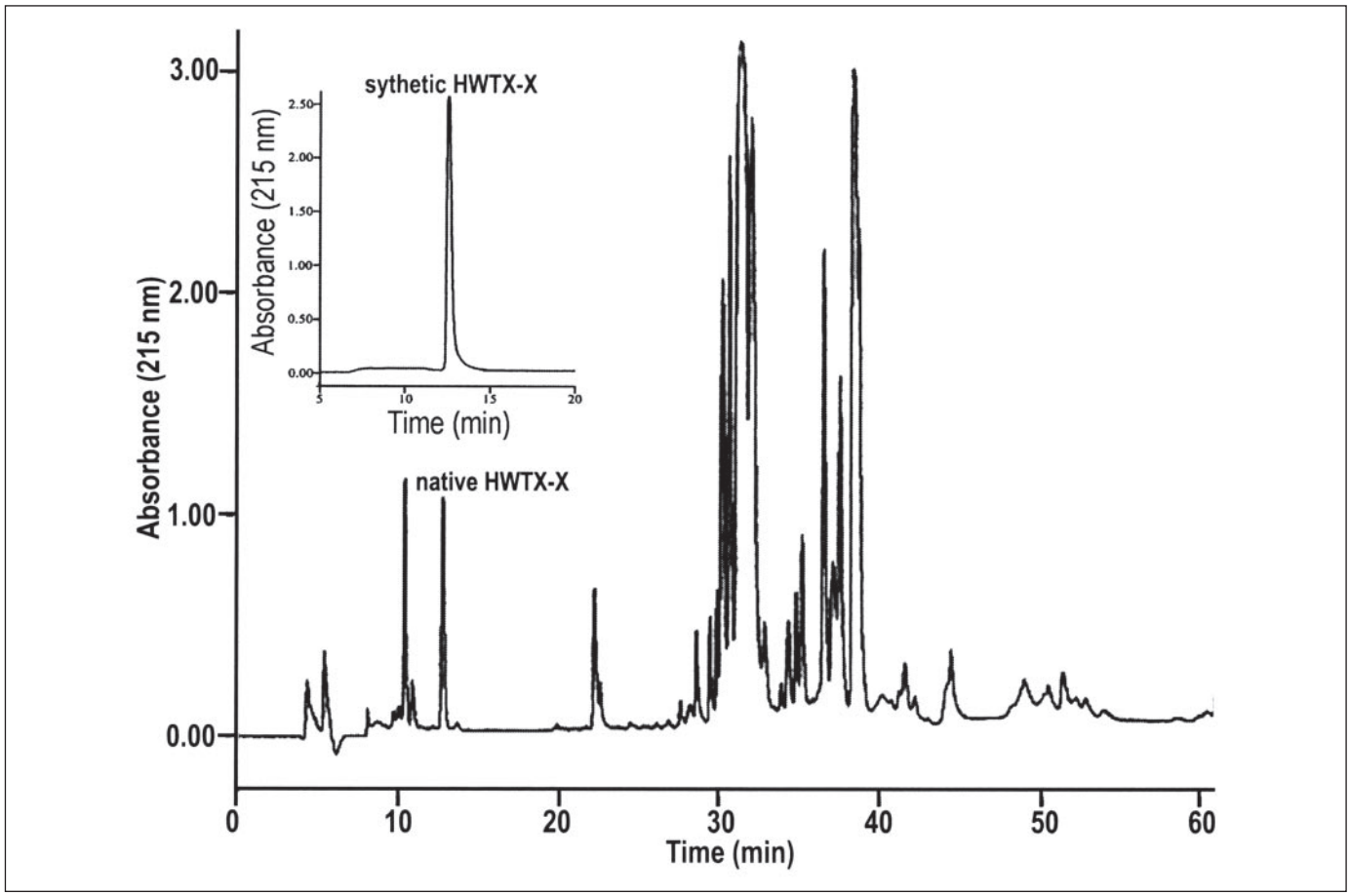

FIGURE 1. **HPLC chromatography of the spider *O. huwena* venom on a Vydac C18 column (4.6 mm × 250 mm).** The peptides were eluted using a linear acetonitrile gradient (0–60% acetonitrile, 0.1% trifluoroacetic acid in 60 min) at a flow rate of 1.0 ml/min. Elution of peptides was monitored at 215 nm. *Inset*, HPLC of synthetic HWTX-X.

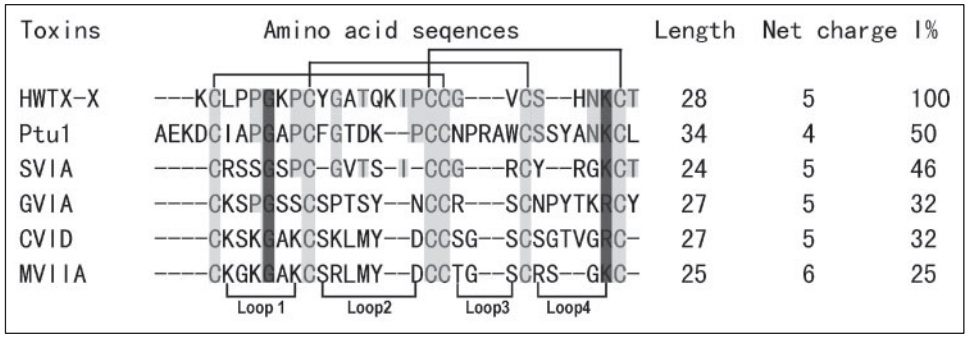

FIGURE 2. **Sequence alignment of HWTX-X with some other toxins active on vertebrate HVA Ca^{2+} channels.** Identical amino acids are shown in *gray* and the two well conserved Gly^6 and Lys^{26}/Arg^{26} are in *black*. The sequence length, net charge, and the percentage identity (*I* %) are shown to the *right* of the sequences. The disulfide linkage and the four loops are indicated *above* and *below* the sequences, respectively.

tion to −50 mV from a holding potential (V_h) of −90 mV, whereas only HVA currents are activated if the cell is depolarized from a V_h of −40 to 0 mV (33–36). Thus, rat DRG cells are appropriate for investigating the effect of HWTX-X on voltage-gated Ca^{2+} channels. As shown in Fig. 4*A*, 10 μM HWTX-X had no discernible effect on T-type Ca^{2+} channels, but it could eliminate 41.4 ± 4.1% of the HVA currents (Fig. 4*B*). From the current-voltage (*I-V*) curves of the HVA currents (Fig. 4*C*), it was found that HWTX-X caused no change on the initial activated voltage, the active voltage of peak inward current, and the reversal potential of the HVA currents.

The HVA currents in rat DRG cells were described as mainly N-type (sensitive to GVIA) and L-type (sensitive to nifedipine) (34). In this study, of the HVA currents, 41.7 ± 3.7% (N-type currents) could be blocked by a saturating concentration of 4 μM GVIA, whereas 40 ± 5.4% (L-type currents) could be reduced by 10 μM nifidipine and then the remaining currents (P/Q- and R-types) were abolished by 25 μM Ni^{2+}. In the presence of 4 μM GVIA, 10 μM HWTX-X had no additional effect on the HVA currents, whereas the addition of nifidipine could inhibit another fraction of the currents that remained, and the currents resistant to these were finally eliminated by adding $NiCl_2$ (Fig. 4*D*). Analogously, after blockage by HWTX-X, GVIA could not cause further blockage (Fig. 4*E*). These results indicated that HWTX-X could specifically block the GVIA-sensitive, N-type Ca^{2+} currents in rat DRG cells. When HWTX-X and MVIIA were compared, we found that after pretreatment with 10 μM HWTX-X, 3.2 μM MVIIA continued to block a small proportion of the remaining currents (Fig. 4*F*), in agreement with previous studies showing that MVIIA at high concentrations can bind the P/Q-type Ca^{2+} channels with low affinity (13, 23).

```
gttattcccg taatttgtaa atcggagaac ggtctgtctg atcaaccaca cagctacttc agacgggaaa
ATG AAC ATG AAA ATA CTT GTT TTA GTT GCC GTC CTT TGT CTG GTT GTC TCT ACT CAT GCT
 M   N   M   K   I   L   V   L   V   A   V   L   C   L   V   V   S   T   H   A
GAA|AGA CAT AGC AAA ACT GAC ATG GAA GAC ATG GAA GAC TCC CCG ATG ATT CAA GAG AGA
 E |R   H   S   K   T   D   M   E   D   M   E   D   S   P   M   I   Q   E   R
  AAG TGT TTA CCA CCG GGC AAA CCT TGT TAC GGA GCA ACA CAG AAG ATT CCG TGC TGC GGA
  K   C   L   P   P   G   K   P   C   Y   G   A   T   Q   K   I   P   C   C   G
GTG TGT TCA CAT AAT AAG TGT ACC TAA ccggcg ggaactattt taaaaagatg ttaactaagg
 V   C   S   H   N   K   C   T  End
aagatgatat gcaatcacat ctgtaaatgga agaagatttc atcgtggaga tatcgggtta ctagatttac
tcttgtaaca ctgtacgctaa attcaaaatt atgattaaac gttatgaata aacagaaaaa aaaaaaaa
```

FIGURE 3. **The oligonucleotide sequence of HWTX-X cDNA.** The amino acid composition of the precursor reading from the cDNA is *below* the nucleotide sequence. The potential endoproteolytic sites are indicated with *down arrows*. The signal sequence is shown in *gray*, the propeptide is *boxed*, and the mature peptide is *underlined*.

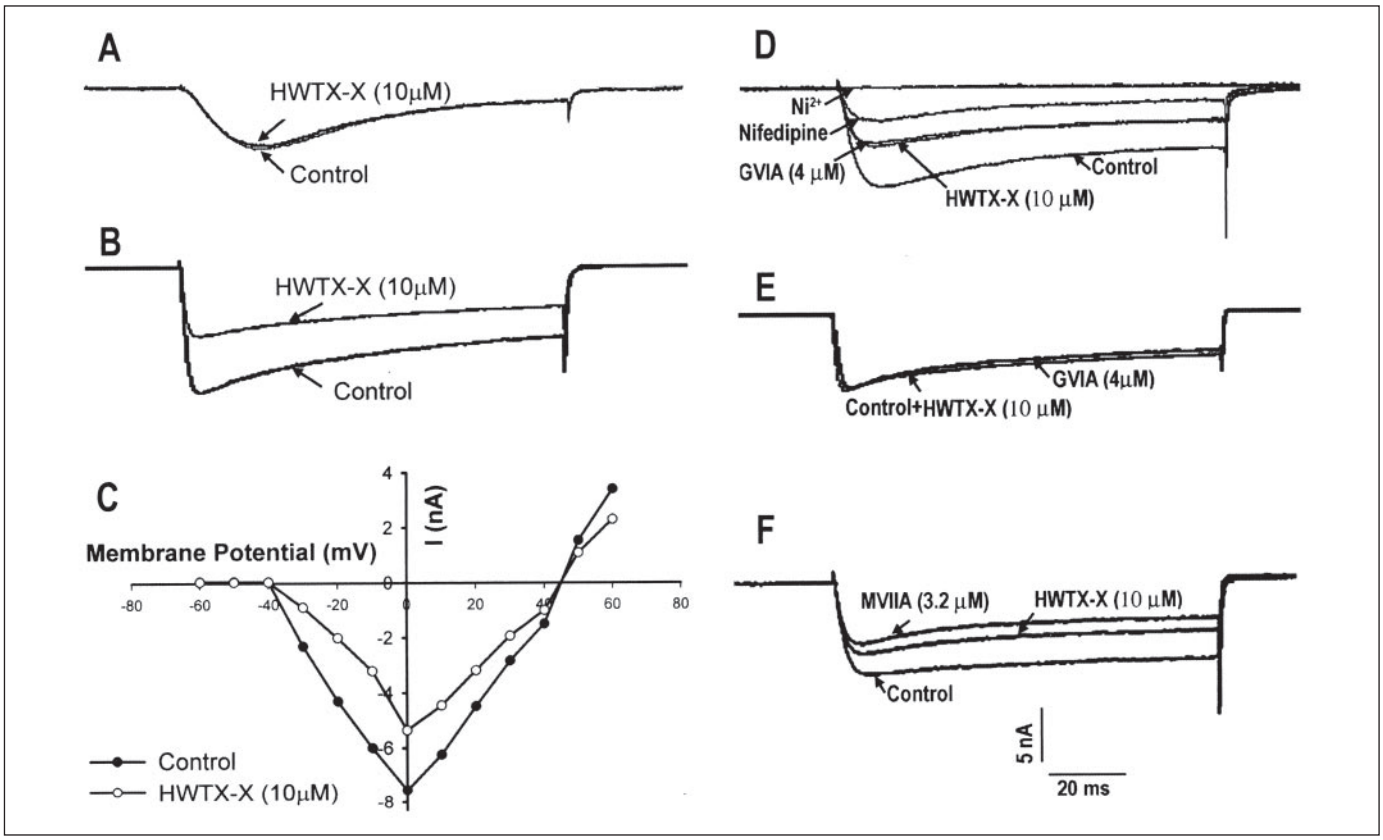

FIGURE 4. **Effect of HWTX-X on Ca^{2+} channels in DRG cells.** *A*, HWTX-X (10 μM) has no significant effect on the low voltage-activated Ca^{2+} channels. *B*, it can partially block the HVA Ca^{2+} channels. *C*, current/voltage (*I*/*V*) relationship for the same cell under control conditions and after addition of 10 μM HWTX-X to the bath. *D*, in the presence of 4 μM GVIA, 10 μM HWTX-X has no additional effect on the HVA currents, whereas the addition of nifidipine and $NiCl_2$ can inhibit the currents that remained. *E*, 4 μM GVIA has no effect on HWTX-X-resistant currents. *F*, MVIIA can block a small proportion of these currents.

Based on the specificity of HWTX-X, GVIA was used to isolate the N-type currents in DRG cells. In each cell tested, 4 μM GVIA was finally added to produce maximal blockage of N-type currents, and then the proportion of blockage by HWTX-X was normalized. HWTX-X could block N-type currents in a dose-dependent manner, which yielded an IC_{50} value of about 40 μM (Fig. 5*A*). Analysis of the dose-response data also revealed a 1:1 binding association of HWTX-X with the channels. The rate of onset of 10 μM HWTX-X blockage was rapid (τ_{on} = 17.4 ± 1.1 s), but it was relatively slower than those of GVIA and MVIIA (τ_{on} = 12.4 ± 0.2 and 12.9 ± 0.3 s). The blockage by HWTX-X could be reversed by washing, with a recovery of ~90% of the control currents within 2 min, whereas the currents blocked by MVIIA were recovered only to ~40% upon a 4-min wash. By contrast, there was little recovery from GVIA blockage of N-type currents (Fig. 5B). 4 μM GVIA could produce additional blockage of N-type currents after pretreatment with 100 nM HWTX-X, but the rate of blockage by GVIA was significantly slowed (τ_{on} = 37 ± 3 s) (Fig. 5*C*). This raised the possibility that the slow blockage was because of the slow replacement of the reversible blocker by the irreversible toxin, suggesting therefore that the two toxins may be directly competing for overlapping (or partially overlapping) binding sites of N-type channels. The effect of HWTX-X on voltage-gated Na^+ and K^+ channels was also assessed in rat DRG cells according the method described by Liu *et al.* (37), which indicated that 10 μM HWTX-X had no effect on the two channels (data not shown).

Disulfide Determination and Structure Calculations of HWTX-X—Sequence-specific resonance assignments were performed according to the standard procedures established by Wüthrich (38). All of the backbone protons and more than 95% of the side chain protons were identified. The four Pro residues (Pro^4, Pro^5, Pro^8, and Pro^{17}) were assigned clearly by the strong sequential Hα-Hδ cross-peaks for Xxx-Pro, which also indicated the presence of trans-peptide bonds for these residues.

As described above, the six Cys residues of HWTX-X are involved in three disulfide bridges. In the absence of chemical characterization, the disulfide linkage of HWTX-X was first speculated from its identical Cys

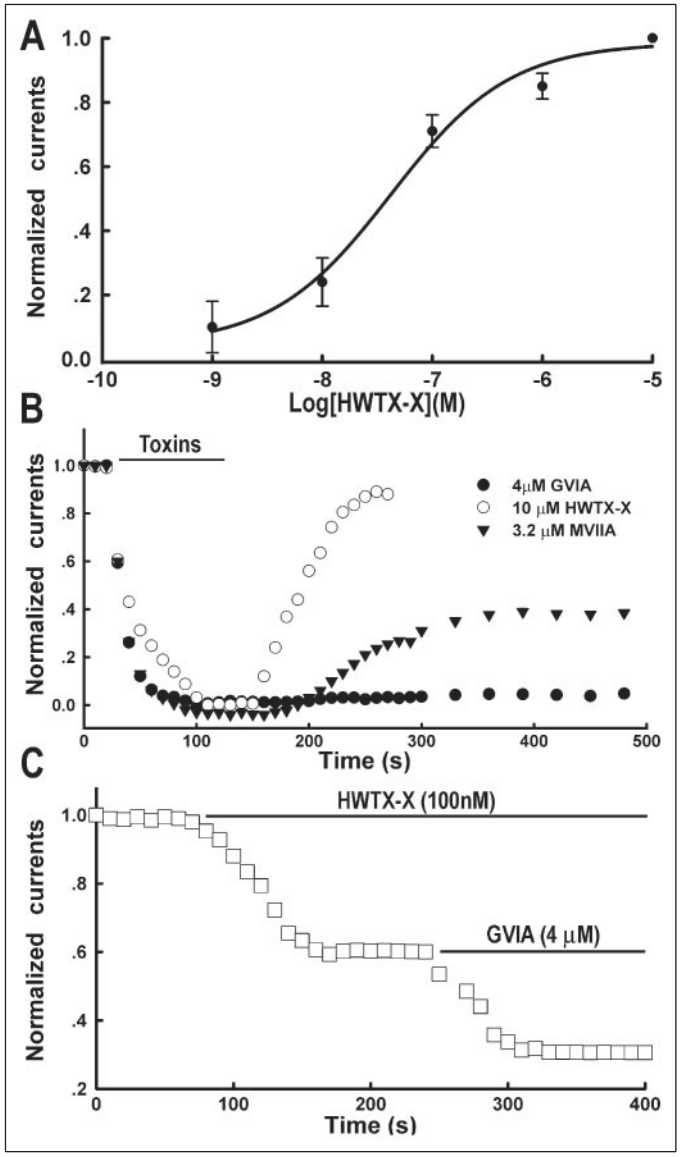

FIGURE 5. *A*, dose-dependent blockage of GVIA-sensitive, N-type Ca^{2+} channels by HWTX-X in DRG cells. *B*, blockage of Ca^{2+} channels by HWTX-X is rapid but slower than those of GVIA and MVIIA. HWTX-X blockage is completely reversible upon a 2-min wash, and MVIIA blockage can be partially recovered, whereas the currents exhibit little recovery after GVIA blockage. *C*, pretreatment of HWTX-X affects the time course of the subsequent blockage by GVIA.

residues motif with those of ω-contoxins. Furthermore, these covalent links could also be identified from the Hα-Hβ and Hα-Hβ NOE contacts observed between the Cys residues involved in the linkage. The NOESY spectra (mixing time of 200 ms) of HWTX-X allowed us to detect several inter-cystinyl NOE cross-peaks (HA Cys^2-HB Cys^{19}, HB Cys^{18}-HA Cys^{27}, and HB Cys^{18}-HB Cys^{27}), and therefore to identify unambiguously the two disulfide bridges: Cys^2–Cys^{19} and Cys^{18}–Cys^{27}. The third disulfide bridge (Cys^9–Cys^{22}) could then be deduced indirectly as the only one possible. Accordingly, disulfide linkage was determined as the I–IV, II—V, and III–VI pattern, which is frequently found in a variety of toxic and inhibitory peptides from biologically diverse sources (39, 40).

The structure of HWTX-X was determined by using 261 intramolecular distance constraints, 10 dihedral constraints as well, as nine distance constraints derived from the three disulfide bridges. Altogether, the final experimental set corresponded to 10 restraints per residue on average. A family of 20 accepted structures with lower energies and better Ramachandran plots were selected to represent the three-dimensional solution structure of HWTX-X. The structures have no distance violations greater than 0.3 Å and no dihedral violations greater than 5.0°. They have favorable non-bonded contacts as evidenced by the low values of the mean Lennard-Jones potentials and good covalent geometry as indicated by the small deviations from ideal bond lengths and bond angles. Analysis of the structures in PROCHECK shows that 77.4% of non-Pro, non-Gly residues lie in the most favored regions of the Ramachandran plot with a further 20.8% in additionally allowed regions. The best fit superposition of the backbone atoms (N, C_α, and C) for the 20 converged structures of HWTX-X gives an average root mean square deviation with respect to mean structure values of 0.93 ± 0.25 Å for backbone atoms and 1.67 ± 0.28 Å for all heavy atoms. The N-terminal residue (Lys^1) and loop 2 region (Gly^{11}–Pro^{17}) show some apparent deviations among the obtained structures. For the remaining part of the structures (2–10 and 18–28), average root mean square deviation values were 0.57 ± 0.13 Å for backbone and 1.25 ± 0.23 Å for heavy atoms.

Structure Description of HWTX-X—A sausage representation of the backbone atoms of the 20 best converged structures of HWTX-X is shown in Fig. 6*A*. The three-dimensional structure of HWTX-X (Protein Data Bank code 1Y29) contains a compact disulfide-bonded core, from which four loops emerge (Leu^3–Pro^8, Tyr^{10}–Pro^{17}, Gly^{20}–Val^{21}, and Ser^{25}–Thr^{28}) as well as N and C termini. Fig. 6*B* shows the ribbon representation of the secondary structure in HWTX-X. The main element of the secondary structure is a short triple-stranded antiparallel β-sheet formed by strands Lys^7–Pro^8, Cys^{22}–Ser^{23}, and Lys^{26}–Cys^{27}, which are stabilized by the three disulfide bridges. Of the 28 residues of HWTX-X, only the side chains of the six Cys residues are buried, all the others are solvent accessible, and their conformations are constrained by steric interactions.

HWTX-X adopts an inhibitor cystine knot motif commonly observed in other toxic and inhibitory peptides (39, 40). The cystine knot in HWTX-X is formed by three disulfide bridges linked as Cys^2–Cys^{19}, Cys^9–Cys^{22}, and Cys^{18}–Cys^{27} in which the Cys^{18}–Cys^{27} disulfide bridge passes through a 12-residue ring formed by the intervening polypeptide backbone and the Cys^2–Cys^{19} and Cys^9–Cys^{22} disulfide bridges. A comparison of the structures of HWTX-X and GVIA highlights a common fold adopted by both peptides (Fig. 6*B*) (41). The structural alignment by using *the combinatorial extension* (*CE*) *method* shows the root mean square deviation value between the structures of HWTX-X and GVIA as 2.1 Å. Similarly, they both contain a cystine knot and a triple-stranded, anti-parallel β-sheet. However, because HWTX-X has dissimilar loop sizes with GVIA (Fig. 2), structural comparison between them also reveals some significant difference, most notably in loop 2. HWTX-X has a larger loop 2, and therefore the two additional residues in loop 2 make this loop structurally more undefined and Lys^{15} protruding from the surface of HWTX-X in this loop (the solvent accessible surface of this residue is more than 68%).

DISCUSSION

In the present study, we have isolated a novel specific blocker of N-type Ca^{2+} channels from the venom of *O. huwena*, which was named HWTX-X. HWTX-X contains 28 amino acid residues, which is the smallest peptide among the huwentoxins so far isolated; it is also similar in size to ω-conotoxins (24–29 residues). This peptide was chemically synthesized and folded to be indistinguishable from the native one. In analogy to ω-conotoxins, HWTX-X contains three disulfide bridges, and is basic. Inspection of the sequences shown in Fig. 2 reveals a con-

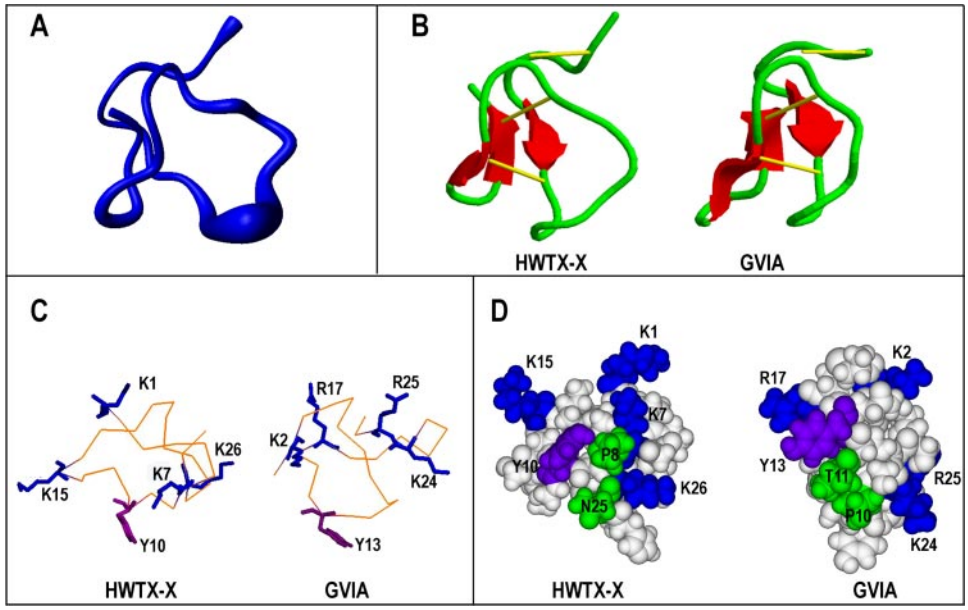

FIGURE 6. *A*, a sausage representation of the backbone atoms of the 20 best converged structures of HWTX-X. *B*, Richardson-style diagrams of the backbone folding of HWTX-X and GVIA. The β-sheet is shown in *red*, and three disulfide bonds of each molecule are indicated in *yellow*. *C*, repartition of basic residues (in *blue*) on the structures of HWTX-X and GVIA. The critical aromatic residue is shown in *purple*. *D*, CPK representation of HWTX-X and GVIA shows seven putative residues in the binding surfaces of both peptides.

served cysteine framework and two conserved residues, Gly^{6} and Lys^{26}/Arg^{26} (HWTX-X numbering), although HWTX-X shows low sequence homology (<32%) with ω-conotoxins other than SVIA. Compared with ω-conotoxins, HWTX-X has a larger loop 2, which demonstrates significant structural differences among those peptides. Cloning and sequencing of the mRNA transcripts from the venom duct of this spider confirmed that HWTX-X is expressed in this tissue. Similarly to other spider peptide toxins and ω-conotoxins, HWTX-X is expressed as a prepropeptide that is post-translationally processed to yield the mature toxin. In contrast to ω-conotoxins GVIA, MVIIA, and CVID, the C terminus of HWTX-X is not amidated.

Previous studies have shown that GVIA and MVIIA are potential blockers of N-type Ca^{2+} channels in various species and nerval tissues by physical occlusion of the pore of their receptors. Consequently, GVIA and MVIIA have become commonly used tools for isolation and identification of native N-type Ca^{2+} channels (4–6). Our studies in rat DRG cells demonstrate that HWTX-X can specifically block the HVA Ca^{2+} currents through GVIA-sensitive, N-type Ca^{2+} channels, whereas it has no detectable effect on the other Ca^{2+} channels, or on the voltage-gated Na^{+} and K^{+} channels. From the current-voltage (I–V) curves of the HVA currents, it has been found that HWTX-X can only suppress peak currents without affecting the kinetics of N-type Ca^{2+} channels, which distinguishes HWTX-X from ω-aga-IVA. ω-Aga-IVA, a peptide isolated from the venom of the funnel web spider *Agelenopsis aperta*, inhibits Ca^{2+} channels by altering the voltage dependence of gating (42, 43). In the present study, the dose-response data indicates that HWTX-X blocks N-type Ca^{2+} channels in a 1:1 manner. Pretreatment of HWTX-X also affects the time course of the subsequent blockage by GVIA, suggesting that HWTX-X should share overlapping (or partially overlapping) binding sites with GVIA. However, HWTX-X is distinct from GVIA or MVIIA in several aspects. MVIIA partially blocks HWTX-X-resistant Ca^{2+} currents, but GVIA does not, which indicates that HWTX-X have specificity similar to GVIA, but it should be more specific than MVIIA for N-type channels. In comparison, GVIA is a poorly reversible blocker and the blockage by MVIIA is only partially recovered, whereas the blockage by HWTX-X is nearly completely reversible. In addition, HWTX-X cannot affect the twitch response of rat vas deferens, whereas GVIA and MVIIA can. It has been reported that GVIA-sensitive, N-type Ca^{2+} channels mediated noradrenergic release in vas deferens at low frequency electrical stimulation (3). Thus, it appears that these N-type Ca^{2+} channels in vas deferens are resistant to HWTX-X, and HWTX-X would be a useful tool to discriminate these iosforms of N-type Ca^{2+} channels.

The structure and function relationships of GVIA have been widely analyzed by using Ala-scanning mutagenesis (32, 44–46). All those studies have shown that Tyr^{13} in loop 2 is the most critical residue for the binding to N-type Ca^{2+} channels. Also, several other residues including Lys^{2}, Arg^{17}, Tyr^{22}, and Lys^{24} have been identified to have a secondary effect on potency. Additional residues with less importance are Hyp^{10}, Thr^{11}, Asn^{20}, Arg^{25}, and Tyr^{27}. On the other hand, utilizing a chimeric combined with site-directed mutagenesis, Ellinor and co-workers (47) demonstrated that the large putative extracellular loop between IIIS5 and IIIH5 was critically important for the block of N-type Ca^{2+} channels by GVIA. In particular, residues Gln^{1327}, Glu^{1334}, Glu^{1337}, and Gln^{1339} of this region were identified as being important for blockage by GVIA, with Glu^{1337} having the largest effect (47). Furthermore, Feng *et al.* (48) found two additional residues, Gly^{1326} and Glu^{1332}, to be important determinants for GVIA blockage. Therefore, it is proposed that the complex between N-type Ca^{2+} channels and GVIA involves the critical aromatic residue (Tyr^{13}) as well as several basic residues that make hydrogen bonds and salt bridges with the corresponding residues located in the pore region of N-type Ca^{2+} channels (30).

HWTX-X shares the same pharmacological specificity and action mechanism in rat DRG cells as GVIA and therefore they might be expected to present similar interacting surface profiles. The determination of the three-dimensional structure of HWTX-X would be helpful to elucidate this point. HWTX-X adopts a common structure fold to GVIA, but it is widely accepted that this overall three-dimensional scaffold generally provides little insight into bioactivities. The cystine knot simply provides the structure framework on which the bioactivity related residues are grafted. Therefore, the topological distribution of the key functional residues of GVIA, regardless of the three-dimensional scaffold, may be instructive for mapping the bioactive surface of HWTX-X. Molecular surface analysis of GVIA reveals that the interacting surface of GVIA encompasses the crucial aromatic residue (Tyr^{13}) surrounded by some basic residues (Lys^{2}, Arg^{17}, Lys^{24}, and Arg^{25}) (Fig. 6*C*), as described by Bernard *et al.* (30). Such a functional motif is also found in HWTX-X, in which the aromatic residue is Try^{10}, and the basic

residues are Lys^{1}, Lys^{7}, Lys^{15}, and Lys^{24}. Like Tyr^{13} of GVIA, residue Tyr^{10} of HWTX-X extrudes from the molecular surface (the solvent accessible surface of Tyr^{10} is about 52.4%, whereas that of Tyr^{13} of GVIA is about 59.4%) and is located in the center of the interacting surface (Fig. 6, *C* and *D*). However, HWTX-X and GVIA are different in some other respects, which highlights some important differences in their bioactive surfaces. These key residues are not in homologous positions when the amino acid sequences are aligned. For example, Tyr^{13} of GVIA is at the ending of loop 2, whereas Tyr^{10} of HWTX-X is at the beginning of the same loop (Fig. 2), which results in reverse spatial orientation of those residues. In addition, HWTX-X lacks the two additional important binding residues Hyp^{10} and Thr^{11} that are close to Tyr^{13} in GVIA. It has been proposed that Pro^{8} and Asn^{25} could compensate for them, but they occupy different spatial positions (Fig. 6*D*). Therefore, similar functional motifs of HWTX-X and GVIA may indicate that they should interact with the same macrosite in N-type Ca^{2+} channels, their differences may involve the different selectivity of HWTX-X for isoforms of N-type Ca^{2+} channels, compared with GVIA.

In summary, HWTX-X specifically blocks GVIA-sensitive, N-type Ca^{2+} channels in rat DRG cells. Its non-toxic effects, specificity, and complete reversibility make it an interesting lead drug for designing novel drugs for the treatment of N-type Ca^{2+} channel-related diseases. A common functional motif between HWTX-X and GVIA may contribute to the similarities in their bioactivities, but the obvious differences of their binding surfaces may explain their different selectivities for iosforms of N-type Ca^{2+} channels. Mutants of HWTX-X are being developed to test the importance of these hypothetical bioactivity-related residues.

Acknowledgments—We are grateful to Guangzhong Tu of Beijing Institute of Microchemistry for collecting the ^{1}H NMR spectra. We thank Prof. Jinyun Xie and Ping Chen for expert assistance and helpful discussions of this work.

REFERENCES

1. Catterall, W. A. (2000) *Cell Dev. Biol.* **16,** 521–555
2. Hofmann, F., Biel, M., and Flockerzi, V. (1994) *Annu. Rev. Neurosci.* **17,** 399–418
3. Olivera, B. M. (1994) *Annu. Rev. Biochem.* **63,** 823–867
4. Olivera, B. M., Gray, W. R., Zeikus, R., McIntosh, J. M., Varga, J., Rivier, J., Santos, V., and Cruz, L. J. (1985) *Science* **230,** 1338–1343
5. Cruz, L. J., and Olivera, B. M. (1985) *J. Biol. Chem.* **261,** 6230–6233
6. Olivera, B. M., Rivier, J., Scottll, J. K., Hillyard, D. R., and Cruz, L. J. (1991) *J. Biol. Chem.* **266,** 22067–22070
7. Lin, Z., Haus, S., Edgerton, J., and Lipscombe, D. (1997) *Neuron* **18,** 153–166
8. Kaneko, S., Cooper, C. B., Nishioka, N., Yamasaki, H., Suzuki, A., Jarvis, S. E., Akaike, A., Satoh, M., and Zamponi, G. W. (2002) *J. Neurosci.* **22,** 82–92
9. Altier, C., and Zamponi, G. W. (2004) *Trends Pharmacol. Sci.* **25,** 465–470
10. Malmberg, A. B., and Yaksh, T. L. (1995) *Pain* **60,** 83–90
11. Garber, K. (2005) *Nat. Biotechnol.* **23,** 399
12. Adams, D. J., Smith, A. B., Schroeder, C. I., Yasuda, T., and Lewis, R. J. (2003) *J. Biol. Chem.* **278,** 4057–4062
13. Lewis, R. J., Nielsen, K. J., Craik, D. J., Loughnan, M. L., Adams, D. A., Sharpe, I. A., Luchian, T., Adams, D. J., Bond, T., Thomas, L., Jones, A., Matheson, J.-L., Drinkwater, R., Andrews, P. R., and Alewood, P. F. (2000) *J. Biol. Chem.* **275,** 35335–35344
14. Smith, M. T., Cabot, P. J., Ross, F. B., Robertson, A. D., and Lewis, R. J. (2002) *Pain* **96,** 119–127
15. Penna, R. D., and Paice, J. A. (2000) *Pain* **85,** 291–296
16. Corzoa, G., Adachi-Akahane, S., Nagao, T., Kusui, Y., and Nakajima, T. (2001) *FEBS Lett.* **499,** 256–261
17. Peng, K., Chen, X. D., and Liang, S. P. (2001) *Toxicon* **39,** 491–498
18. Tedford, H. W., Sollod, B. L., Maggio, F., and King, G. F. (2004) *Toxicon* **43,** 601–618
19. Liang, S. (2004) *Toxicon* **43,** 575–585
20. Shu, Q., and Liang, S. P. (1999) *J. Pept. Res.* **53,** 486–491
21. Shu, Q., Lu, S. Y., Gu, X. C., and Liang, S. P. (2002) *Protein Sci.* **11,** 245–252
22. Peng, K., Shu, Q., Liu, Z., and Liang, S. P. (2002) *J. Biol. Chem.* **277,** 47564–47571
23. Lu, S. Y., Liang, S. P., and Gu, X. C. (1999) *J. Protein Chem.* **18,** 609–617
24. Diao, J., Lin, Y., Tang, J., and Liang, S. (2003) *Toxicon* **42,** 715–723
25. Li, D., Xiao, Y., Xu, X., Xiong, X., Lu, S., Liu, Z., Zhu, Q., Wang, M., Gu, X., and Liang, S. (2004) *J. Biol. Chem.* **279,** 37734–37740
26. Liang, S. P., Chen, X. D., Shu, Q., Zhang, Y., and Peng, K. (2000) *Toxicon* **38,** 1237–1246
27. Hu, H. Z., and Li, Z. W. (1997) *J. Physiol.* **501,** 67–75
28. Hertz, A., Hernandez, J. F., Gagnon, J., Hong, T. T., Pham, T. T., Nguyen, T. M., Le-Nguyen, D., and Chiche, L. (2001) *Biochemistry* **40,** 7973–7983
29. Schwieters, C. D., Kuszewski, J. J., Tjandra, N., and Clore, G. M. (2003) *J. Magn. Res.* **160,** 66–74
30. Bernard, C., Corzo, G., Mosbah, A., Nakajima, T., and Darbon, H. (2001) *Biochemistry* **40,** 12795–12800
31. Ramilo, C., Zafaralla, G. C., Nadasdi, L., Hammerland, L. G., Yoshikami, D., Gray, W. R., Kristipati, R., Ramachandran, J., Miljanich, G., Olivera, B. M., and Cruz, L. J. (1992) *Biochemistry* **31,** 9919–9926
32. Lew, M. J., Flinn, J. P., Pallaghy, P. K., Murphy, R., Whorlow, S. L., Wright, C. E., Norton, R. S., and Angus, J. A. (1997) *J. Biol. Chem.* **272,** 12014–12023
33. Scroggs, R. S., and Fox, A. P. (1992) *J. Physiol.* **445,** 639–658
34. Miller, R. J. (1987) *Science* **235,** 46–52
35. Miller, R. J. (1992) *J. Biol. Chem.* **267,** 1403–1406
36. Nowychy, M. C., Fox, A. P., and Tsien, R. W. (1985) *Nature* **316,** 440–443
37. Liu, Z., Dai, J., Chen, Z., Hu, W., Xiao, Y., and Liang, S. (2003) *Cell Mol. Life Sci.* **60,** 972–978
38. Wüthrich, K. (1986) *NMR of Protein and Nucleic Acids*, John Wiley & Sons, Inc., New York
39. Pallaghy, P. K., Nielsen, K. J., Craik, D. J., and Norton, R. S. (1994) *Protein Sci.* **3,** 1833–1839
40. Gelly, J. C., Gracy, J., Kaas, Q., Le-Nguyen, D., Heitz, A., and Chiche, L. (2004) *Nucleic Acids Res.* **32,** 156–159
41. Mould, J., Yasuda, T., Schroeder, C. I., Beedle, A. M., Doering, C. J., Zamponi, G. W., Adams, D. J., and Lewis, R. J. (2004) *J. Biol. Chem.* **279,** 34705–34714
42. Isabelle, M. M., Virginia, J. V., Michael, E. A., and Bruce, P. E. (1991) *Proc. Natl. Acad. Sci. U. S. A.* **88,** 6628–6631
43. Sidach, S. S., and Mintz, I. M. (2000) *J. Neurosci.* **20,** 7174–7182
44. Nielsen, K. J., Schroeder, T., and Lewis, R. (2000) *J. Mol. Recognit.* **13,** 55–70
45. Kim, J. I., Takahashi, M., Ogura, A., Kohno, T., Kudo, Y., and Sato, K. (1994) *J. Biol. Chem.* **269,** 23876–23878
46. Nadasdi, L., Yamashiro, D., Chung, D., Tarczyhornoch, K., Adriaenssens, P., and Ramachandran, J. (1995) *Biochemistry* **34,** 8076–8081
47. Ellinor, P. T., Zhang, J. F., Horne, W. A., and Tsien, R. W. (1994) *Nature* **372,** 272–275
48. Feng, Z. P., Hamid, J., Doering, C., Bosey, G. M., Snutch, T. P., and Zamponi, G. W. (2001) *J. Biol. Chem.* **276,** 15728–15735
49. Hansson, K., Ma, X., Eliasson, L., Czerwiec, E., Furie, B., Furie, B. C., Rorsman, P., and Stenflo, J. (2004) *J. Biol. Chem.* **279,** 32453–32463